Journal of Physics and Chemistry of Solids 200 (2025) 112618

Contents lists available at ScienceDirect

Journal of Physics and Chemistry of Solids

journal homepage: www.elsevier.com/locate/jpcs

First-principles calculations to investigate structural, electronic, mechanical, optical, vibrational, thermal properties, and hydrogen storage capabilities of Rb_2SnH_4 for hydrogen storage applications

Cengiz Soykan [a], Cihan Kürkçü [b,*]

[a] Department of Medical Services and Techniques, Kırşehir Ahi Evran University, Kırşehir, Türkiye
[b] Department of Electronics and Automation, Kırşehir Ahi Evran University, Kırşehir, Türkiye

ARTICLE INFO

Keywords:
Hydrogen storage
Electronic properties
Elastic properties
Optical properties
Vibrational properties
Thermal properties

ABSTRACT

The structural, electronic, mechanical, optical, vibrational, and thermal properties of tetragonal Rb_2SnH_4 belonging to the space group $P4_2/mnm$ as a hydrogen storage material, were meticulously examined using the ab initio method. The gravimetric hydrogen densities were determined as 2.77 wt%. The hydrogen desorption temperatures were measured at 29.05 K for Rb_2SnH_4. Electronic band structure computations yielded band gap values of 0.455 eV. The elevated band gap values indicate that Rb_2SnH_4 possesses semiconductor properties. The values of the second-order independent elastic constants, which indicate the hardness and mechanical stability of the materials, were computed. The values of the elastic constants indicated that Rb_2SnH_4 exhibits mechanical stability. Hardness characteristics, including bulk modulus, shear modulus, B/G ratio, Young's modulus, and Poisson's ratio, were computed utilizing the values of elastic constants. Based on the B/G ratio (1.764), Rb_2SnH_4 was identified as ductile material. Based on Poisson's ratio (0.262), the atoms in Rb_2SnH_4 compounds are interconnected by ionic bonds. Besides, the vibrational properties were also analyzed, and Rb_2SnH_4 is also dynamically stable as it has no negative branches. Furthermore, several optical parameters of Rb_2SnH_4, including dielectric function, conductivity, reflectivity, and absorption, were computed. Finally, the thermo-physical characteristics of this compound were computed.

1. Introduction

The study of hydrogen storage materials as a renewable energy source is becoming increasingly important as they offer sustainable, clean, and efficient solutions for energy production and consumption. While hydrogen has great potential as a clean energy carrier, its effective and safe storage is a critical issue for the success of energy systems. Renewable energy sources such as wind and sun are intermittent in nature; that is, they do not produce energy continuously. Hydrogen is seen as a way of storing excess energy from these intermittent sources for later use. Efficient storage of hydrogen helps to address imbalances between energy production and demand. Hydrogen produces only water vapor when burned or used in fuel cells, so it does not cause harmful carbon emissions into the environment. As an alternative to fossil fuels, hydrogen is a clean energy carrier. However, because hydrogen gas is very light and has a low volumetric energy density, effective storage methods need to be developed. The storability of hydrogen makes its use in portable energy systems possible. Especially in the transportation sector, hydrogen-fueled vehicles (fuel cell vehicles) can greatly reduce carbon emissions. The development of hydrogen storage technologies enables more widespread and safer use of such portable energy sources. Hydrogen is used not only in the energy sector but also in many industrial processes. Hydrogen plays a critical role in the chemical, metallurgical, and petrochemical industries. Hydrogen storage materials are important to increase efficiency and provide environmentally friendly solutions in these sectors. Making the storage and utilization of hydrogen independent of fossil fuels contributes greatly to reducing carbon emissions and environmental impacts. Studies on hydrogen storage materials are key to the transition to greener energy systems that minimize carbon emissions [1–7].

Moreover, this study positions Rb_2SnH_4 as a promising material for next-generation hydrogen storage technologies, meeting the growing demand for clean, efficient, and sustainable energy solutions. Its unique combination of thermal, mechanical, and electronic properties makes it

* Corresponding author.
E-mail address: ckurkcu@ahievran.edu.tr (C. Kürkçü).

https://doi.org/10.1016/j.jpcs.2025.112618
Received 1 December 2024; Received in revised form 11 January 2025; Accepted 3 February 2025
Available online 7 February 2025

versatile for a variety of energy-related applications. Applications include portable fuel cells, automotive hydrogen storage, residential energy systems, hydrogen-powered vehicles, grid-level backup systems, and industrial processes.

There are many different structures as hydrogen storage materials. For example, double perovskites are very much studied in this field. Double perovskites generally exhibit high thermodynamic stability. This is critical for the safe storage and long-term preservation of hydrogen. This structure can provide resistance to chemical degradation in the absorption and desorption processes of hydrogen. Double perovskites generally have high gravimetric and volumetric hydrogen storage capacities. This feature is especially advantageous for portable energy systems and mobile applications [8–12]. In addition, there are a large number of studies on physical properties such as structural, electronic, and elastic properties of materials used in many fields of technology. However, it is a fact that studies on hydrogen storage properties will reduce the world's need for fossil fuels [13–22].

As a result of the literature review, there is no previous study on the Rb2SnH4 compound that we can compare. This study will be the first study on the physical properties of the Rb2SnH4 compound. The primary objective of this study is to evaluate the hydrogen storage potential of the Rb_2SnH_4 compound and to examine its suitability as a sustainable hydrogen storage material for the energy sector. In this context, the structural, electronic, mechanical, optical, vibrational, and thermal properties of Rb_2SnH_4 have been thoroughly investigated. The study aims to reveal the stability, energy efficiency, and application potential of the compound through theoretical analyses. The motivation for this research stems from the growing significance of hydrogen as a clean energy carrier and the critical need for safe and efficient storage methods for the success of energy systems. Particularly, the intermittent nature of renewable energy sources exacerbates the need for solutions that can balance energy production and demand. Hydrogen serves as a vital tool for storing surplus energy and utilizing it when required. However, challenges such as hydrogen gas's low density and energy intensity necessitate the development of effective storage technologies. In this study, Rb_2SnH_4's structural stability, mechanical resilience, electronic band structure, optical properties, thermal behaviors, and hydrogen storage capacity have been analyzed in detail. Furthermore, the compound's dynamic and thermodynamic stability has been evaluated through various physical properties and hydrogen adsorption/desorption processes. The analyses demonstrate that Rb_2SnH_4 is a promising candidate for efficient hydrogen storage in renewable energy systems. This study contributes to the development of hydrogen storage technologies and aims to provide sustainable energy solutions that reduce carbon emissions.

2. Calculations

All total-energy calculations were conducted using the CASTEP software, which relies on Density Functional Theory (DFT) and employs the plane-wave pseudopotential method [23–26]. The exchange-correlation function was characterized by the generalized gradient approximation (GGA), as developed by Perdew, Burke, and Ernzerhof (PBE) [27]. For geometry optimization across all crystal structures, pseudopotentials were employed with an energy cutoff set at 650 eV in total energy and stress calculations.

In calculations involving crystalline structures, it is typically sufficient to perform periodic functions of the Bloch wave vector throughout the entire or specified parts of the Brillouin zone (BZ). However, to enhance computational efficiency, especially in complex calculations where computational demand is substantial for each BZ point, these functions are calculated at a carefully chosen subset of BZ points [28]. The reciprocal space was sampled using a Monkhorst-Pack 6 × 6 × 9 k-point grid, optimized for the unit cell geometry. Ultrasoft pseudopotentials were utilized to represent the interactions between ionic cores and valence electrons. The valence electron configurations were set as follows: Rb $4s^2\ 4p^6\ 5s^1$, Sn 4 $d^{10}\ 5s^2\ 5p^2$, and H $1s^1$. Geometric optimization calculations employed the Broyden–Fletcher–Goldfarb–Shanno (BFGS) minimization algorithm with ultra-fine quality, establishing convergence tolerances for electronic self-consistency, energy, maximum force, maximum stress, and maximum atomic displacement at $1.0x10^{-6}$ eV/atom, 0.01 eV/Å, 0.02 GPa, and $1.0x10^{-4}$ Å, respectively [29]. Subsequently, optical and phonon properties were calculated through single-point energy calculations using norm-conserving pseudopotentials. We employed the Vesta program [30], which provides us with a wealth of information regarding the compounds under investigation, such as their atomic positions, space groups, and lattice parameter values.

3. Results and discussion

3.1. Structural properties

The crystal structure of the tetragonal type Rb_2SnH_4 compound with space group *P42/mnm* is given in Fig. 1. There are 24 atoms in the unit cell. Rb atoms are located at Wyckoff positions 4a (0,0,0,0) while Sn atoms are located at positions 3 b (0,0,0,0). H atoms are located at Wyckoff position 4c (0,0,0,0).

The lattice parameter values obtained for the Rb_2SnH_4 compound are given in Table 1. Since the physical properties of this compound were calculated for the first time in this study, no comparison could be made in the table.

In addition, the formation energy value was also calculated to reveal whether the *P42/mnm* phase of the Rb_2SnH_4 compound is thermodynamically stable. As a result of the calculations, the formation energy for this structure was obtained as −0.034 using equation (1).

$$\Delta H_f = \frac{1}{(n_{Rb}+n_{Sn}+n_{H_2})}\left[E_{tot}(Rb_2SnH_4) - n_{Rb}E_{tot}(Rb) - n_{Sn}E_{tot}(Sn) - n_{H_2}E_{tot}(H_2)\right] \quad (1)$$

Whereas E_{H2} indicates the total energy of the hydrogen molecule, E_{Rb} and E_{Sn} stand for the total energy of the ground state of the Rb and S elements in bulk form, respectively. n_{Rb}, n_{Sn} and n_{H_2} refer to the number of *Rb*, *Sn*, and *H* atoms in the unit cell. E_{tot} (Rb_2SnH_4) indicates the total energy of Rb_2SnH_4. The formation energy value obtained for Rb_2SnH_4 is

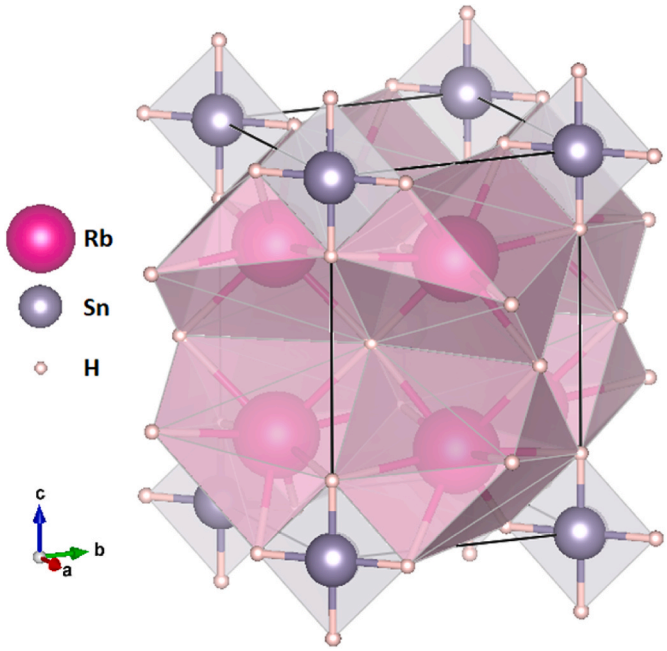

Fig. 1. The crystal structure of Rb_2SnH_4.

Table 1
The lattice parameters of Rb_2SnH_4.

Material	Lattice Constans (A^0), a, b, c	Volume (A^3)	$\Delta E_f(eV/atom)$	$G_{wt}(\%)$	Refs.
Rb_2SnH_4	6.218, 6.218, 8.818	340.989	−0.034	2.77	This Study
	6.018, 6.018, 8.710	315.444	–	–	OQMD

negative. This means that the structure is thermodynamically stable and can be synthesized in the experimental setting.

3.2. Electronic properties

Calculations of the electronic band structure are crucial for determining whether a material is a conductor, semiconductor, or insulator, and for optimizing the design and performance of electronic devices. A material's electronic band structure defines the energy difference (band gap) between the conduction bands and the valence bands. This difference determines the material's electrical conductivity. In conductors, the band gap is close to zero, while in semiconductors there is a specific energy difference. In insulators, however, the band gap is much wider. The band structure of materials also affects their optical properties, such as the absorption or emission of photons. Therefore, band structure calculations are important for designing optoelectronic devices. Additionally, in energy technologies such as solar cells, batteries, thermoelectric materials, and hydrogen storage, the electronic band structure of materials plays a critical role in efficiency and performance.

In Fig. 2, the band structure and density of states (DOS) of the Rb_2SnH_4 compound are presented. The Fermi energy level is set to 0 eV and is indicated by the red dashed line. There is a band gap of 0.455 eV between the maximum of the valence band and the minimum of the conduction band. This indicates that the Rb_2SnH_4 compound exhibits semiconducting characteristics in the *P*42/*mnm* phase. The fact that the band gap is this small indicates that the material can be excited with low energy and may operate in the infrared region. Additionally, the maximum of the valence band and the minimum of the conduction band are located at the same symmetry point (G), which corresponds to a direct band gap semiconductor.

The band gap value of 0.455 eV for Rb_2SnH_4 indicates semiconducting behavior, which not only suggests the potential for optoelectronic applications but also carries significant implications for hydrogen storage performance. The relatively small band gap enables electronic excitation with low energy input, which can influence both desorption kinetics and the thermal properties of the material. In hydrogen storage systems, the electronic structure of the material plays a critical role in determining the energy barrier for hydrogen desorption. The semiconducting nature of Rb_2SnH_4, combined with its direct band gap, facilitates electron excitation under moderate thermal or optical stimulation. This property can lower the activation energy required for hydrogen desorption, enabling efficient hydrogen release at lower temperatures. This feature is particularly advantageous for applications where energy efficiency is a priority, such as portable fuel cells or grid-scale energy storage systems. Additionally, the band gap's influence extends to the thermal properties of the material. The electronic contributions to thermal conductivity, mediated by the band gap, affect how heat is distributed within the material during adsorption and desorption cycles. A small band gap can enhance the material's ability to dissipate heat efficiently, reducing the risk of localized overheating that could lead to structural degradation or performance inconsistencies. This thermal stability supports the material's robustness and longevity in industrial applications. The semiconducting characteristics of Rb_2SnH_4 also present opportunities for coupling hydrogen storage with optoelectronic technologies. For instance, integrating Rb_2SnH_4 into systems where hydrogen production and storage are driven by solar energy could leverage its electronic properties to optimize performance under light exposure. By bridging the band gap's implications to hydrogen desorption kinetics and thermal management, Rb_2SnH_4 is further validated as a multifunctional material with the potential to advance both energy storage and conversion technologies.

In Fig. 2, the total density of states is similar to the band structure. Below the Fermi energy level between (0 eV)-(-1.2 eV), the largest contribution comes from the Sn-p orbital. Between (−1.2 eV)-(-2.6 eV) and after −4 eV, the largest contribution comes from the H-s orbital.

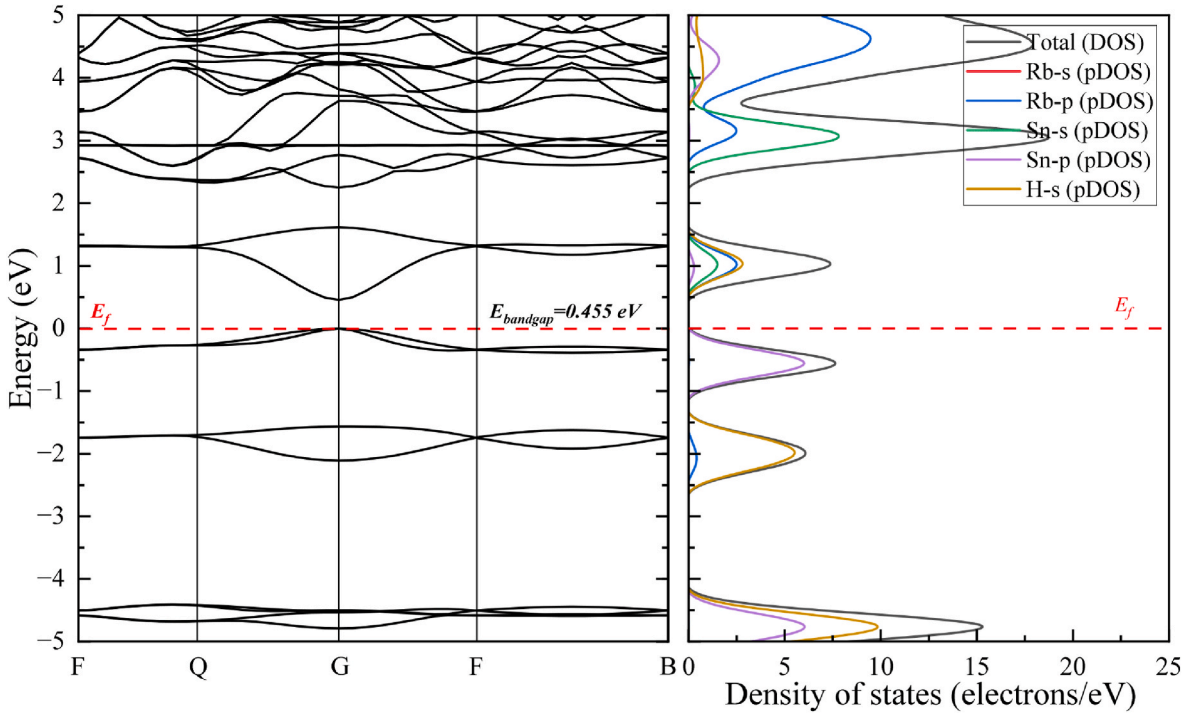

Fig. 2. The electronic band structure and density of states for the *P*42/*mnm* phase of Rb_2SnH_4.

Above the Fermi energy level (0 eV)-(1.6 eV) the largest contribution comes from the H-s orbital. Between (2.5 eV)-(3.5 eV) the largest contribution comes from the Sn-s orbital, while at (3.5 eV) and above it comes from the Rb-p orbital.

3.3. Mechanical properties

The calculation of elastic properties is of great importance for understanding the mechanical performance and behavior of materials. Elastic constants determine how a material will respond to stress, strain, or deformation. Table 2 shows the values of the elastic constants of certain materials (C_{11}, C_{12}, C_{13}, C_{33}, C_{44} and C_{66}) in GPa. These data include the mechanical properties of the compound Rb_2SnH_4 and how this compound is characterized by calculations obtained from density functional theory (GGA-PBE).

Born stability criteria for tetragonal crystal structures are mathematical conditions used to determine the elastic stability of the crystal structure. These criteria must be met to ensure the elastic stability of a material. Stability conditions are established using certain combinations of elastic constants (Cij) in a tetragonal crystal structure.

Born criteria for elastic stability in tetragonal crystals must satisfy the following conditions [31]:

$$C_{11} > 0, C_{33} > 0, C_{44} > 0, C_{66} > 0, (C_{11} - C_{12}) > 0$$

$$(C_{11} + C_{13} - 2C_{13}) > 0, (2C_{11} + C_{33} + 2C_{12} + 4C_{13}) > 0 \quad (1)$$

Born stability criteria for tetragonal crystal structures ensure the elastic stability of the structure in different directions. These conditions help determine whether the crystal can remain stable under strain and mechanical stress. If these criteria are not met, the structure becomes mechanically unstable, and cracking, fracture, or anisotropic deformations can occur. This condition guarantees that the deformations in all three dimensions of the material are consistent and balanced against each other. The tetragonal-type structure of Rb_2SnH_4 is mechanically stable, as all elastic constant values obtained in this study satisfy these Born stability criteria.

In order to have more information about the hardness and strength of the material, some hardness parameters were also calculated using elastic constant values, as shown in Table 3.

Bulk modulus (B) is the resistance of a material to volumetric compression. It can be calculated using elastic constants as follows:

$$B = \frac{C_{11} + 2C_{12}}{3} \quad (2)$$

Bulk modulus indicates how long the material will retain its volume under external forces. A high bulk modulus indicates that the material is less compressible, i.e. it is stiff.

The shear modulus (G) describes the resistance of a material to shear forces. It is calculated using elastic constants C44 and C66:

$$G = \frac{C_{44} + C_{66}}{2} \quad (3)$$

The shear modulus indicates how resistant the material is to shear stresses. A higher shear modulus means that the material is stiffer.

Poisson's ratio indicates the amount of transverse expansion of a material under an axial load. It can be calculated using elastic constants. For tetragonal structures, the Poisson's ratio can be expressed as follows:

Table 2
Second order independent elastic constant values for the tetragonal structure of Rb2SnH4.

Composition (GPa)	C_{11}	C_{12}	C_{13}	C_{33}	C_{44}	C_{66}
Rb_2SnH_4	18.474	5.239	6.354	17.521	5.551	5.183

Table 3
Bulk moduli B, shear moduli G, Young's modulus E (all in GPa), Pugh's ratio B/G, anisotropic factor A, and Poisson's ratio υ for the tetragonal structure of Rb2SnH4.

Composition (GPa)	B	G	E	B/G	A	υ
Rb_2SnH_4	10.040	5.692	14.362	1.764	0.839	0.262

$$\nu = \frac{C_{12}}{C_{11} + C_{12}} \quad (4)$$

Poisson's ratio allows us to understand how the material deforms and the volume changes during elastic deformation. Poisson's ratio also gives us information about the bonds that the atoms that make up the material make with each other. If Poisson's ratio is around 0.1, the atoms in the material make covalent bonds with each other. If this value is around 0.25, we can talk about ionic bonding. However, if the Poisson's ratio is as high as 0.3–0.5, weak bonds such as metallic bonds are formed in the material. Since the Poisson's ratio obtained in this study is 0.262, the atoms are connected to each other by ionic bonds.

Young's modulus is a parameter that measures how much a material stretches or deforms under axial stress.

This modulus determines how stiff or flexible the material is. A higher Young's modulus indicates that the material is stiffer. In this study, Young's modulus value was obtained as 14.362.

The Zener anisotropy ratio is a measure that determines whether a material is anisotropic or not. For isotropic materials, this ratio is 1. If the Zener ratio is different from 1, it means that the material exhibits different elastic behavior in different directions (anisotropic). Since the anisotropy ratio obtained in this study is different from 1, the material is anisotropic.

The Pugh ratio is a measure used to determine whether a material is brittle or ductile. It is found by the ratio of the bulk modulus to the shear modulus: B/G.

If the B/G ratio is greater than 1.75, the material is considered ductile, if it is smaller, it is considered brittle. This ratio shows how much deformation a material can undergo before fracture. Since the B/G ratio obtained in this study is greater than 1.75, the tetragonal-type structure of Rb_2SnH_4 has ductile properties.

As a result, the calculation of elastic properties plays a critical role when developing new alloys, compounds, or materials. Predictions by computational methods (such as GGA-PBE) allow for predicting the performance of the material before experiments. This speeds up experimental processes and reduces costs.

3.4. Optical properties

Fig. 3 shows a plot of the real and imaginary parts of the dielectric function versus frequency. The real and imaginary parts of the dielectric constant have distinct physical meanings and provide insight into the interaction between electromagnetic waves and a material. The real part (ε_1) represents the material's ability to store electrical energy or how it polarizes in response to an applied electric field. It describes the dispersive behavior of the material, indicating how the phase velocity of light changes as it propagates through the medium. The imaginary part (ε_2) represents energy dissipation or absorption within the material when subjected to an electromagnetic field. It is a measure of the material's absorptive behavior and quantifies how much energy from the field is lost as heat.

The interaction of a medium with light at varying photon energies is characterized by the complex dielectric function ($\varepsilon = \varepsilon_1 + i\varepsilon_2$). The maximum value of the real part (ε_1) of this function is linked to electron excitation. The imaginary component (ε_2) of the complex dielectric function can be determined through the momentum matrix elements derived from the occupied and unoccupied states. Additionally, the real part (ε_1) can be obtained from the imaginary part (ε_2) via the Kramer-

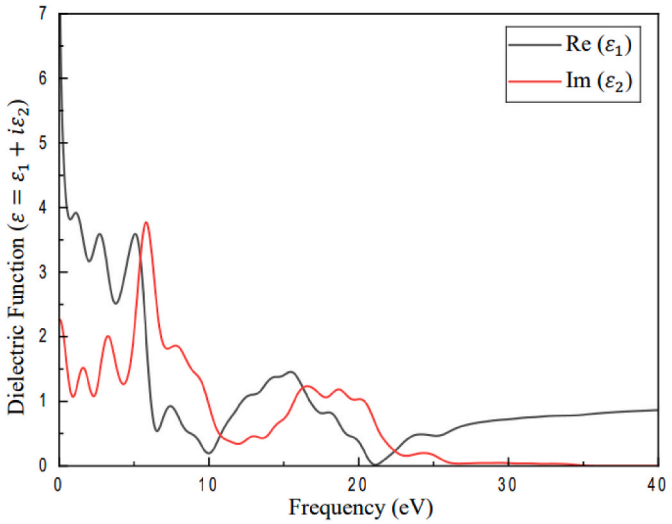

Fig. 3. The optical dielectric function for the *P*42/*mnm* phase of Rb_2SnH_4. The calculations are for polycrystalline form.

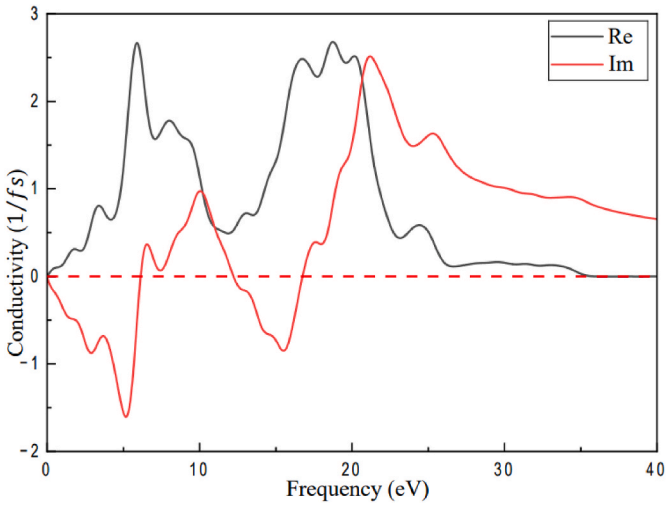

Fig. 4. The optical conductivity (1/*fs*) for the *P*42/*mnm* phase of Rb_2SnH_4. The calculations are for polycrystalline form.

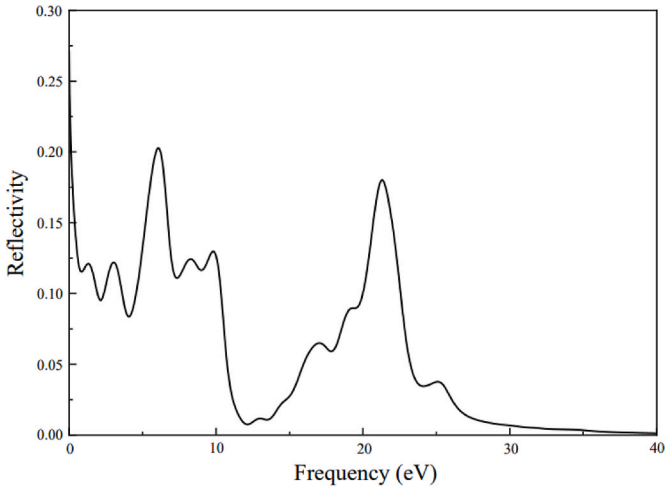

Fig. 5. The optical reflectivity for the *P*42/*mnm* phase of Rb_2SnH_4. The calculations are for polycrystalline form.

Kronig relation. In this context, the real part (ε_1) of the dielectric function demonstrates dispersive behavior, while the imaginary part (ε_2) shows absorptive characteristics. Both components are presented as a function of frequency (eV) in Fig. 3. In particular, Fig. 3 highlights that, for the Rb_2SnH_4 phase, the highest peak of the imaginary part (ε_2) in the UV region occurs within the range of approximately 4.40 eV–7.24 eV, corresponding to a wavelength of 5.82 eV. Additional peaks are observed at 3.26 eV and 1.58 eV, respectively.

The variation of the frequency-dependent conductivity properties of Rb_2SnH_4 is presented in Fig. 5. In the low-frequency region (0–5 *eV*), the conductivity values are close to zero but not exactly zero, indicating that the material behaves like a semiconductor. This result supports the band gap value of 0.455 *eV* that we calculated from the electronic band gap calculation. As the frequency increases, it is observed that the optical conductivity increases, reaching a maximum value of 2.66 (1/ *fs*) at a frequency of 5.90 *eV*. This point represents a significant photon absorption region where the material's photon absorption is at its highest. Additionally, this peak value corresponds to the material's natural resonance frequency. Since conductivity is at its maximum, the material can absorb more energy or electrons can be excited more easily around this frequency. As the frequency increases, two more peaks are observed at frequency values of 16 and 18 *eV*. At these points, there is additional electron mobility in the material. Conductivity will relatively increase at these values as well. After a frequency of 20 *eV*, the material's conductivity rapidly approaches zero. This indicates that the electrons' ability to be excited decreases due to changes in the material's energy levels. After a frequency of 35 *eV*, the energy levels of the material are structured in such a way that they hinder the free movement of electrons. As a result, the material's capacity to interact with high-energy photons decreases, and it becomes insulating.

When examining Fig. 4, it is observed that the lowest peak point of the imaginary part of the curve corresponds to a frequency of 5.14 *eV*. This negative imaginary peak value indicates that, at the frequency of 5.14 *eV*, losses are minimal while conductivity is quite high. This result is highly consistent with the highest peak value of the real part at a frequency of 5.9 *eV*. Both peak values demonstrate that, in this frequency region, optical absorption or, in other words, electron mobility is significantly high. As the frequency increases, another negative-valued imaginary peak is present at the frequency region of 15.51 *eV*. This point represents a frequency region where losses that would reduce the material's optical absorption are low. This is further supported by the increasing real peak. At a frequency of 21.14 *eV*, the imaginary part reaches a positive peak value. This indicates that, in this region, losses increase, conductivity decreases, and the material becomes increasingly insulating. This behavior is also supported by the rapidly decreasing real part after a frequency of 20.16 *eV*.

As seen in Fig. 5, reflectivity decreases in the low-frequency range up to a frequency value of 4.11 *eV*. At a frequency of 4.11 *eV*, there is a maximum loss of reflectivity in the material. In this region, light absorption has increased. This behavior is consistent with the increasing conductivity values in this range. The increasing reflectivity peak at 6.08 *eV* indicates a decrease in conductivity. The frequency value of 6.08 *eV* corresponds to the decreasing region following the first maximum value of the conductivity peak at 5.90 *eV*.

In this region, the increase in reflectivity is consistent with the decrease in conductivity. At a frequency of 12.17 *eV*, reflectivity reaches its lowest value. The decrease in reflectivity in this area aligns with the increase in conductivity in the frequency range of 12.08–20.20 *eV*. As reflectivity decreases in this region, photon absorption increases. Beyond the 20.20 eV region, the optical conductivity of Rb_2SnH_4 decreases sharply, approaching near-zero values, while the reflectivity exhibits a rapid increase, indicating a transition where the material becomes more reflective and less conductive at higher photon energies.

As can be seen from Fig. 6, there is a fluctuation in the absorbance value. There is a gradual increase from the low-frequency region to the

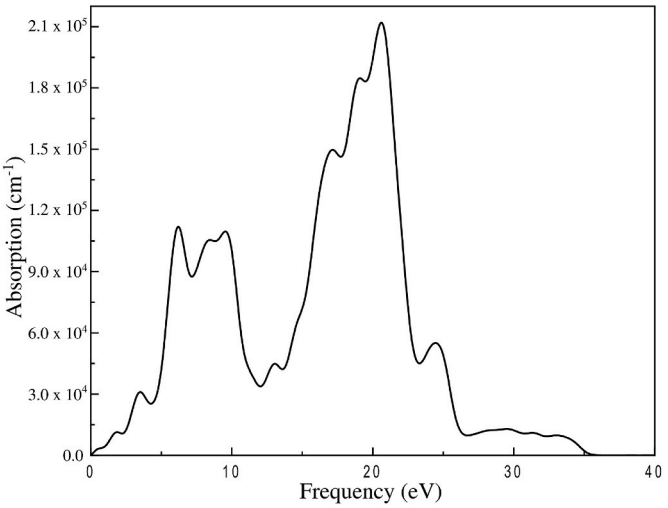

Fig. 6. The optical absorption (cm^{-1}) for the *P*42/*mnm* phase of Rb_2SnH_4. The calculations are for polycrystalline form.

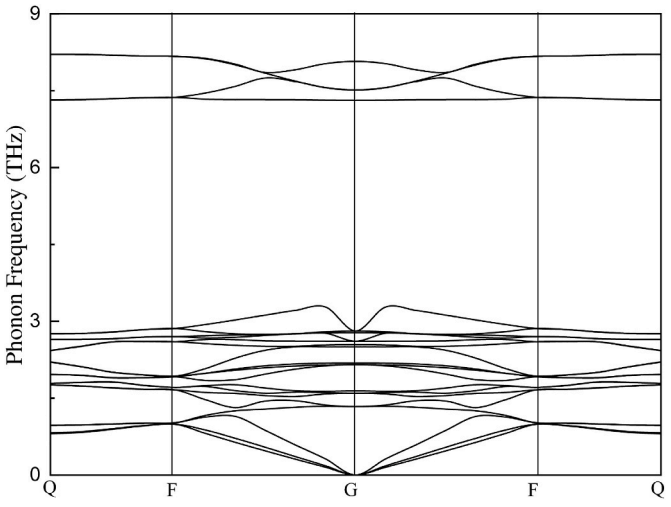

Fig. 7. The phonon dispersion curve for the *P*42/*mnm* phase of Rb_2SnH_4.

high-frequency region, with the first peak value corresponding to a frequency of approximately 6.19 *eV*. At this point, a high level of photon absorption occurs, and this point is one of the natural resonance points of the material. As seen in Fig. 4, the high conductivity value at this point (approximately 2.34 1/*fs*) also supports this result.

In the mid-frequency region, the absorbance value continues to increase from a frequency of 12.04–20.54 *eV*. In this region, the material exhibits the highest absorbance behavior. When compared to the conductivity graph in Fig. 4, it is observed that the material's conductivity reaches its highest values in this region. The results of absorbance and conductivity support each other in the mid-frequency region. After approximately 20.51 *eV*, both conductivity and absorbance properties decrease rapidly. This indicates that high-frequency photons can no longer be absorbed, and conductivity decreases rapidly.

Optical properties such as conductivity and reflectivity are critical for understanding the interaction of electromagnetic fields with hydrogen storage materials. For instance, these properties influence the material's thermal behavior under irradiation and its energy efficiency in storage systems exposed to varying environmental conditions. In the case of Rb_2SnH_4, the observed optical parameters suggest potential benefits in thermal management, which could stabilize hydrogen adsorption and desorption processes over a wide temperature range.

3.5. Vibrational properties

Phonon calculations of materials, especially in solid state physics, are performed to understand and model the thermal and dynamic properties of materials. Phonons are quasi-particles resulting from vibrations of atoms in the crystal structure, and these vibrations determine various physical properties of materials.

A **phonon** is a quantum mechanical concept used to describe the collective vibrational motion of atoms in a crystal lattice. It is a quasi-particle that represents the quantized energy of lattice vibrations. Phonons arise from the periodic arrangement of atoms in a crystal lattice vibrating around their equilibrium positions. These vibrations are collective and propagate as waves through the lattice. Phonons are composed of two parts: acoustic and optical. Acoustic Phonons represent low-energy vibrations where atoms oscillate in a coherent wave-like manner, similar to sound waves. These phonons dominate heat conduction in solids. Optical Phonons arises in crystals with more than one atom per unit cell, where atoms oscillate out of phase with each other. These phonons are essential in optical and infrared absorption processes.

The distribution of acoustic and optical modes along the axes of high symmetry for the Rb_2SnH_4 compound is given in Fig. 7. Since there are N = 24 atoms in the unit cell of this structure, it has a total of 3 N, i.e. 72 modes. While 3 of these modes are acoustic modes, the remaining 69 modes correspond to optical modes. Analyzing phonon modes can also help determine whether a crystal structure is stable or not. If phantom (negative frequency) phonons are present in a material, this indicates that the structure is dynamically unstable and may transform into a different structure. If all phonon frequencies are positive, as in this study, this means that the structure is dynamically stable.

The phonon dispersion analysis of Rb_2SnH_4 reveals the absence of negative frequencies, confirming its dynamic stability. This result is crucial as it indicates that the material remains stable against lattice vibrations, a property essential for maintaining structural integrity under various operational conditions. In practical terms, dynamic stability translates to resistance against phase transitions that could compromise hydrogen storage performance. During hydrogen adsorption and desorption cycles, the material is subjected to thermal and mechanical stresses. A dynamically stable material like Rb_2SnH_4 is less likely to undergo unwanted structural transformations, ensuring consistent hydrogen release and uptake across a wide range of operating conditions. This stability is particularly advantageous in industrial settings where materials must perform reliably over extended periods and repeated cycles. For example, in hydrogen storage tanks used in renewable energy grids or fuel cell vehicles, dynamic stability ensures that the material can withstand temperature fluctuations and mechanical vibrations without degradation or phase shifts. The robust phonon stability also implies compatibility with various external conditions, such as pressure changes, which are common in hydrogen storage and distribution systems. Furthermore, the absence of negative phonon frequencies highlights the suitability of Rb_2SnH_4 for scalable applications, as the material can maintain its performance under the more rigorous demands of industrial-scale hydrogen storage. This characteristic contributes to the longevity and cost-effectiveness of storage systems, reducing the need for frequent material replacement or system downtime for maintenance. By confirming dynamic stability, the phonon dispersion analysis supports the broader applicability of Rb_2SnH_4 as a reliable hydrogen storage material in diverse energy systems, reinforcing its potential for advancing sustainable energy solutions.

3.6. Thermal properties

Fig. 8 shows the variation of heat capacity (cal/cell*K) with temperature (K) [32]. In the low-temperature region (0–200 K), the heat capacity is low. However, it increases linearly towards the mid-temperature region (200–400 K). This behavior indicates that the Rb_2SnH_4 material has low atomic mobility in the low-temperature limit,

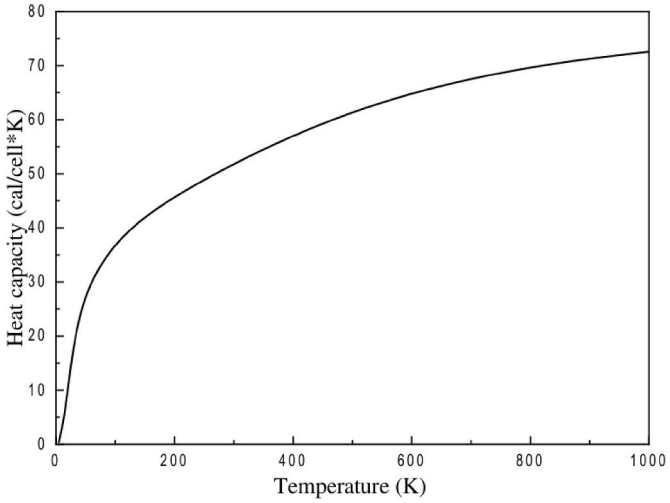

Fig. 8. The heat capacity curve for the *P*42/*mnm* phase of Rb_2SnH_4.

allowing the hydrogen atoms to bind more stably to the material [33, 34]. In the mid-temperature region (200–400 K), it tends to form a plateau by reducing the slope of the linear increase. This structure persists in the high-temperature region, although the slope increases slightly. The behavior of the heat capacity (cal/cell*K) supports the presence of a stable crystal structure in both the mid- and high-temperature limits. As a result, the processes of hydrogen adsorption to or desorption from the structure can be stably repeated over a wide temperature range.

The graph showing the variation of the Debye temperature (Θ_D) with temperature (K) presented in Fig. 9 supports the behavior of heat capacity (cal/cell*K) [35]. In particular, the plateau structure that forms in the mid-temperature and high-temperature limits is an indication of the material's thermal and structural stability, providing evidence that stable and continuous hydrogen storage and release behavior can be repeated over a long period.

3.7. Hydrogen storage properties

The graph of heat capacity (cal/cell*K) versus temperature (K) presented in Fig. 8 provides clues about the hydrogen storage performance of the Rb_2SnH_4 material and the processes of hydrogen adsorption and desorption. In the low-temperature region (0–200 K), although the material's heat capacity is low, it increases steadily. This behavior indicates that the hydrogen adsorption capacity is high due to minimal atomic mobility in this region and that it increases towards the mid-temperature region. In the mid-temperature region (200–400 K), compared to the low-temperature region, the trend of increasing heat capacity decreases, and a plateau-like structure is observed. The slope of this plateau structure decreases as the temperature increases, becoming flatter. This behavior in the mid- and high-temperature regions indicates that the material can be thermally stable over a long temperature range. This region is optimal for the material's hydrogen storage and release, corresponding to a quite wide temperature range. In this region, the stability of the material's crystal structure is high, and the processes of hydrogen storage and release can be stably repeated over a long period. When examining the behavior of the Rb_2SnH_4 material at high-temperature limits (<400 K), while a steady increase in heat capacity is expected, a plateau structure is also observed. This situation indicates that the material's stability continues at high temperatures and that the hydrogen storage and release processes can also proceed. Although hydrogen release may be more challenging in this region according to the behavior of heat capacity, it is advantageous in terms of efficiency. From another perspective, the result indicating a higher hydrogen storage capacity is exciting.

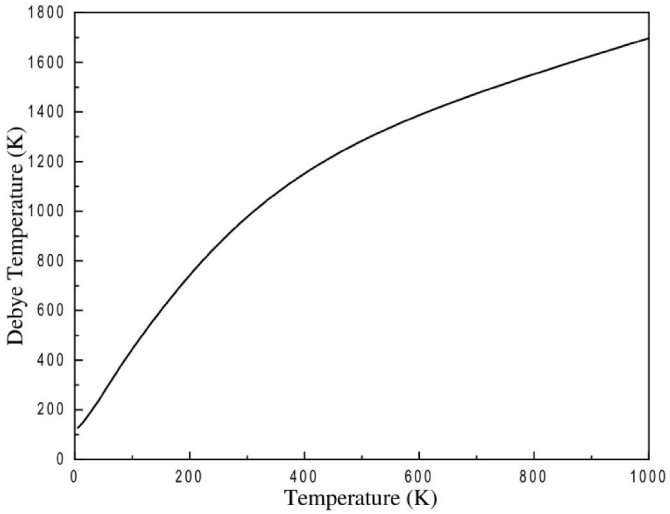

Fig. 9. The Debye temperature curve for the *P*42/*mnm* phase of Rb_2SnH_4.

Fig. 9 shows the variation of the Debye temperature (Θ_D) of the Rb_2SnH_4 material with temperature (K). With increasing temperature, the Debye temperature (Θ_D) also increases steadily [36]. The trend of increase is linear in the low-temperature limit. This behavior is similar to that of heat capacity, indicating that the hydrogen storage capacity is high in this region. As the upper limits of the mid-temperature range are approached, the slope of the increase decreases, forming a plateau structure. Thus, because the material can maintain its thermal and structural stability in the mid-temperature and near-high-temperature limits, a continuous hydrogen storage and release process can be repeated in this region. The behaviors of both the Debye temperature (Θ_D) and heat capacity (cal/cell*K) support each other across all temperature limits.

The stability of the heat capacity and Debye temperature of Rb_2SnH_4 across a broad temperature range is a key indicator of its suitability for repeated hydrogen adsorption and desorption cycles. This characteristic suggests that Rb_2SnH_4 can maintain its structural and thermodynamic integrity under cyclic thermal loads, a critical requirement for industrial hydrogen storage systems. In industrial applications, materials used for hydrogen storage must endure multiple loading and unloading cycles without significant degradation. The consistent heat capacity behavior observed in Rb_2SnH_4 indicates low atomic mobility at lower temperatures, ensuring stable hydrogen bonding. At higher temperatures, the plateau-like behavior supports the idea that hydrogen desorption can occur reliably without compromising the material's structure. These features make Rb_2SnH_4 particularly suitable for systems requiring frequent cycling, such as energy storage in renewable energy grids, where hydrogen acts as a buffer to manage the intermittency of solar and wind power. Additionally, the stable Debye temperature profile suggests that Rb_2SnH_4 can withstand thermal stresses over prolonged operation, minimizing the risk of material fatigue. This stability is essential for large-scale applications, including stationary hydrogen storage for industrial energy management and mobile systems like fuel cell-powered vehicles. The low desorption temperature of Rb_2SnH_4 further enhances its practicality by reducing energy input requirements for hydrogen release, contributing to overall system efficiency. The combination of these properties positions Rb_2SnH_4 as a promising material for integration into next-generation hydrogen storage technologies. Its ability to perform reliably under industrial conditions, coupled with its environmental and safety advantages, underscores its potential to support the transition to a clean energy economy.

The gravimetric storage capacity $G_{wt}(\%)$ of the Rb_2SnH_4 material has been calculated to be 2.77 wt%. The gravimetric storage capacities of magnesium hydride (MgH_2) [37–45], sodium aluminum hydride

($NaAlH_4$) [46,47], lithium borohydride ($LiBH_4$) [48–50], and ammonia borane (NH_3BH_3) [51] are determined to be 7.6, 5.5 (in two steps: 3.7 and 1.8 wt%), 18.5, and 19.6 wt%, respectively.

The gravimetric hydrogen storage capacity of Rb_2SnH_4, calculated as 2.77 wt%, is indeed lower than those of some other hydrides, such as lithium borohydride ($LiBH_4$) with 18.5 wt% and ammonia borane (NH_3BH_3) with 19.6 wt%. However, Rb_2SnH_4 offers several operational advantages that make it a compelling candidate for practical applications despite its comparatively lower capacity. High-capacity materials like $LiBH_4$ and NH_3BH_3 often require elevated temperatures ($LiBH_4$ desorbs at over 300 °C) or high pressures to achieve efficient hydrogen release. These conditions increase the complexity and cost of storage systems and can pose safety risks in industrial and portable applications. In contrast, Rb_2SnH_4 exhibits a much lower desorption temperature (29.05 K), which significantly reduces the energy input required for hydrogen release. This feature enables the design of simpler, more energy-efficient storage systems suitable for a broader range of applications. Unlike NH_3BH_3, which releases toxic ammonia and boron-based compounds during decomposition, Rb_2SnH_4 releases hydrogen without forming harmful by-products. This clean decomposition behavior enhances safety, reduces environmental impact, and simplifies post-release material management, making it an ideal choice for applications in residential or confined spaces.

MgH_2 requires high temperatures for hydrogen release. Similarly, it needs a pressure of 10–50 bar or higher for hydrogen storage. Rb_2SnH_4 is more advantageous in hydrogen release and storage processes due to the early plateau behavior observed in both heat capacity and Debye temperatures. The hydrogen release processes of $NaAlH_4$ occur in two stages (1st stage: 3.7 wt% at 185 °C and 2nd stage: 1.8 wt% at 250 °C) [52]. Additionally, pristine $NaAlH_4$ cannot reabsorb hydrogen [52]. At this point, Rb_2SnH_4 is more advantageous due to its stable thermodynamic structure.

The hydrogen release mechanism of $LiBH_4$ is similar to that of MgH_2. Despite its high storage capacity, it requires high temperatures for hydrogen release. Since this process starts at those temperatures in Rb_2SnH_4, it can provide advantages in practical applications. Lastly, the NH_3BH_3 material has a significantly high gravimetric storage capacity (19.6 wt%) compared to Rb_2SnH_4. However, although it starts releasing hydrogen at low temperatures, it requires high temperatures to reach total release. During the temperature-dependent thermal decomposition of NH_3BH_3, toxic ammonia (NH_3) and boron-based compounds are released. Additionally, the recycling process after hydrogen release from NH_3BH_3 is difficult, and it requires resynthesis. In contrast, no toxic by-products are formed during the thermal transformation of the Rb_2SnH_4 material. Unlike materials such as ammonia borane (NH_3BH_3), which release toxic ammonia (NH_3) and boron-based compounds during decomposition, Rb_2SnH_4 decomposes cleanly without generating harmful emissions. This feature significantly reduces the environmental impact and enhances the material's safety profile for practical applications, particularly in confined or residential settings where the release of toxic gases would pose health risks. Moreover, the clean decomposition of Rb_2SnH_4 contributes to easier recycling and reusability compared to other materials, such as sodium aluminum hydride ($NaAlH_4$). $NaAlH_4$ not only releases hydrogen in multiple steps at high temperatures but also faces challenges in reabsorbing hydrogen, often requiring catalytic enhancements or resynthesis. In contrast, the thermodynamically stable structure of Rb_2SnH_4 allows for repeated hydrogen adsorption and desorption cycles over a broad temperature range, improving operational efficiency and minimizing waste. In terms of safety, materials like magnesium hydride (MgH_2) and lithium borohydride ($LiBH_4$), although they exhibit higher gravimetric storage capacities, require extremely high temperatures and pressures for hydrogen release. These conditions can introduce risks such as system overpressure or thermal instability. Rb_2SnH_4, with its lower desorption temperature (29.05 K) and stable release profile, offers a safer alternative for integration into hydrogen energy systems. Finally, Rb_2SnH_4's environmental compatibility aligns with the broader goals of renewable energy systems, aiming to minimize carbon footprints and hazardous waste. Its clean hydrogen release mechanism makes it a promising candidate for applications where environmental compliance and safety are paramount, such as residential energy storage, portable fuel cells, and automotive technologies.

As seen in Figs. 8 and 9, the early onset of the long plateau curve behavior promises a stable adsorption and desorption process. In this regard, Rb_2SnH_4 could be a good candidate for hydrogen storage materials. Finally, to the best of our knowledge, theoretically, the material's mechanical, electronic, optical, thermal, vibrational, and hydrogen storage properties have been investigated for the first time in this study.

4. Conclusions

This study comprehensively examined the structural, electronic, mechanical, optical, vibrational, thermal, and hydrogen storage properties of the Rb_2SnH_4 compound. The results demonstrate that this material is a promising candidate for hydrogen storage applications. Rb_2SnH_4 exhibits thermodynamic and dynamic stability, as evidenced by its negative formation energy, compliance with Born stability criteria, and positive phonon frequencies. The electronic band structure analysis revealed that the material possesses semiconducting properties with a band gap of 0.455 eV, which supports its potential for low-energy hydrogen desorption and optoelectronic applications. Elastic constant calculations confirm the mechanical stability and ductility of the material, with ionic bonds between the atoms. Additionally, the consistent heat capacity and Debye temperature profile of Rb_2SnH_4 support its durability under repeated thermal and mechanical stresses. In terms of optical properties, the material exhibits significant conductivity and reflectivity, enhancing its potential for integration into energy conversion technologies. Rb_2SnH_4 has a hydrogen storage capacity of 2.77 wt% and can release hydrogen at a low desorption temperature of 29.05 K without producing toxic byproducts. This clean and efficient hydrogen release mechanism makes it suitable for renewable energy applications, portable energy systems, and grid-scale storage.

In conclusion, this study demonstrates that Rb_2SnH_4 is a stable, efficient, and environmentally friendly hydrogen storage material with significant potential for integration into sustainable hydrogen energy systems. Its unique properties contribute to the advancement of clean energy technologies.

CRediT authorship contribution statement

Cengiz Soykan: Writing – review & editing, Writing – original draft, Methodology, Investigation. **Cihan Kürkçü:** Writing – review & editing, Writing – original draft, Supervision, Methodology, Investigation.

Declaration of competing interest

The authors declare that they have no known competing financial interests or personal relationships that could have appeared to influence the work reported in this paper.

Data availability

Data will be made available on request.

References

[1] Q. Hassan, S. Algburi, A.Z. Sameen, H.M. Salman, M. Jaszczur, A review of hybrid renewable energy systems: solar and wind-powered solutions: challenges, opportunities, and policy implications, Res. Eng. (2023) 101621.
[2] Q. Hassan, A.Z. Sameen, H.M. Salman, M. Jaszczur, A.K. Al-Jiboory, Hydrogen energy future: advancements in storage technologies and implications for sustainability, J. Energy Storage 72 (2023) 108404.

[3] M. Balat, Potential importance of hydrogen as a future solution to environmental and transportation problems, Int. J. Hydrogen Energy 33 (2008) 4013–4029.
[4] Ç. Yamçıçıer, C. Kürkçü, Ab initio study of the structural, mechanical, optoelectronic and thermo-physical properties of XGaH5 (X= Ba, Ca, and Mg) compounds for hydrogen storage applications, Int. J. Hydrogen Energy 81 (2024) 391–404.
[5] S. Al, Ç. Yamçıçıer, Computational exploration of hexahydride materials (K2SiH6 and Rb2SiH6); structural, mechanical, thermodynamic, optic, electronic and dynamic properties, J. Energy Storage 91 (2024) 112033.
[6] Ç. Yamçıçıer, C. Kürkçü, Investigation of structural, electronic, elastic, vibrational, thermodynamic, and optical properties of Mg2NiH4 and Mg2RuH4 compounds used in hydrogen storage, J. Energy Storage 84 (2024) 110883.
[7] C. Kurkcu, S. Al, C. Yamcicier, Investigation of mechanical properties of KCaH3 and KSrH3 orthorhombic perovskite hydrides under high pressure for hydrogen storage applications, Eur. Phys. J. B 95 (2022) 180.
[8] M. Caid, D. Rached, H. Rached, Y. Rached, Structural, elastic, electronic, and optical properties of lead-free halide double perovskites Cs2B'B''Br6 (B'B'': BeMg, CdBe, CdGe, GeMg, GeZn, MgZn): ab initio calculations, J. Mol. Model. 30 (2024) 59.
[9] M. Caid, D. Rached, Y. Rached, H. Rached, Comprehensive exploration of halide double perovskites Cs2B'GeCl6 (B': Zn, Cd) for affordable energy technologies: a high-throughput investigation, Opt. Quant. Electron. 56 (2024) 980.
[10] A. Kourdaci, I. Bourachid, H. Bouafia, K. Mecheri, B. Abidri, D. Rached, First-principles calculations to examine structural, magnetic, mechanical, electronic and optical properties of wide bandgap semiconductor Gadolinium Aluminum Oxide perovskite GdAlO3, Comput. Cond. Matter 38 (2024) e00889.
[11] M. Caid, D. Rached, S. Al-Qaisi, Y. Rached, H. Rached, DFT calculations on physical properties of the lead-free halide-based double perovskite compound Cs2CdZnCl6, Solid State Commun. 369 (2023) 115216.
[12] M. Caid, D. Rached, H. Rached, Y. Rached, A density functional theory exploration of Cs2B′ B ″I6 (B′ B ″: BeCa, BeSr, GeCd, GeBe, GeMg) halide double perovskites for optimal solar cell and renewable energy applications, physica status solidi (b) 261 (2024) 2300577.
[13] B. Marzougui, Y.B. Smida, M. Ferhi, H. Ferjani, D. Onwudiwe, A.H. Hamzaoui, M. Triki, Y. Al-Douri, Photoluminescence properties of Pr-doped LaAsO4: an experimental and theoretical study employing density functional theory, Ceram. Int. 50 (2024) 26435.
[14] S. Al-Essa, S.S. Essaoud, A. Bouhemadou, M.E. Ketfi, S. Maabed, F. Djilani, S. Bin-Omran, M. Radjai, D. Allali, R. Khenata, Y. Al-Douri, An ab initio analysis of the electronic, optical, and thermoelectric characteristics of the Zintl phase CsGaSb2, Phys. Scri. 99 (2024) 095996.
[15] Y.B. Smida, B. Marzougui, M. Driss, D.C. Onwudiwe, Y. Al-Douri, Exploring the optoelectronic potential of M2SnX3F2 (M= Sr, Ba; X= S, Se) compounds through first-principles analysis of structural, electronic, and optical properties, Chem. Africa 7 (2024) 491–503.
[16] A. Abdelakader, B. Ahmed, M. Noureddine, B. Mokhtar, Z. Abdelhalim, M. Omar, B. Djillali, A. Yahia, Y. Al-Douri, Theoretical investigations of electronic, thermodynamic and thermoelectric properties of filled skutterudites ThFe4P12 and CeFe4P12 using DFT calculations, Solid State Commun. 380 (2024) 115435.
[17] D. Allali, B. Abdelmadjid, S.E. Saber, D. Bahri, F. Zerarga, R. Amari, M. Radjai, S. Bin-Omran, K. Rabah, Y. Al-Douri, A first-principles investigation on the structural, electronic and optical characteristics of tetragonal compounds XAgO (X= Li, Na, K, Rb), Comput. Cond. Matter 38 (2024) e00876.
[18] H. Allaf, M. Radjai, D. Allali, A. Bouhemadou, S.S. Essaoud, S. Bin-Omran, R. Khenata, Y. Al-Douri, Ab initio predictions of pressure-dependent structural, elastic, and thermodynamic properties of CaLiX3 (X= Cl, Br, and I) halide perovskites, Comput. Cond. Matter 37 (2023) e00850.
[19] D. Allali, R. Amari, A. Bouhemadou, A. Boukhari, B. Deghfel, S.S. Essaoud, S. Bin-Omran, M. Radjai, R. Khenata, Y. Al-Douri, Ab initio investigation of structural, elastic, and thermodynamic characteristics of tetragonal XAgO compounds (X= Li, Na, K, Rb), Phys. Scri. 98 (2023) 115905.
[20] R. Samia, A. Yahia, B. Ahmed, B. Mokhtar, M. Noureddine, L. Mohamed, B. Djillali, Y. Al-Douri, Electronic, elastic and piezoelectric properties calculations of perovskites materials type BiXO3 (X= Al, Sc): DFT and DFPT investigations, Chem. Phys. 573 (2023) 111998.
[21] B. Tahir, A. Bouhemadou, S. Bin-Omran, R. Khenata, Y. Al-Douri, N. Guechi, Ab initio predictions of the structural, electronic, optical, elastic, and thermoelectric properties of quasi-two-dimensional BaFZnP, Comput. Cond. Matter 35 (2023) e00809.
[22] A. Benamara, N. Moulay, Y. Azzaz, M. Ameri, M. Rabah, Y. Al-Douri, A. Bouhemadou, C. Moumen, Elastic, electronic, thermal and magnetic investigations of PrX2 (X= Fe, Ru) superconductors materials, Mater. Today Commun. 35 (2023) 105545.
[23] S.J. Clark, M.D. Segall, C.J. Pickard, P.J. Hasnip, M.I. Probert, K. Refson, M. C. Payne, First principles methods using CASTEP, Z. Kristallogr. Cryst. Mater. 220 (2005) 567–570.
[24] G. Kresse, J. Furthmüller, Efficiency of ab-initio total energy calculations for metals and semiconductors using a plane-wave basis set, Comput. Mater. Sci. 6 (1996) 15–50.
[25] G. Kresse, J. Furthmüller, Efficient iterative schemes for ab initio total-energy calculations using a plane-wave basis set, Phys. Rev. B 54 (1996) 11169.
[26] G. Kresse, J. Hafner, Norm-conserving and ultrasoft pseudopotentials for first-row and transition elements, J. Phys. Condens. Matter 6 (1994) 8245.
[27] J.P. Perdew, K. Burke, M. Ernzerhof, Generalized gradient approximation made simple, Phys. Rev. Lett. 77 (1996) 3865.
[28] H.J. Monkhorst, J.D. Pack, Special points for Brillouin-zone integrations, Phys. Rev. B 13 (1976) 5188.
[29] T.H. Fischer, J. Almlof, General methods for geometry and wave function optimization, J. Phys. Chem. 96 (1992) 9768–9774.
[30] K. Momma, F. Izumi, VESTA: a three-dimensional visualization system for electronic and structural analysis, J. Appl. Crystallogr. 41 (2008) 653–658.
[31] J. Gao, Q.-J. Liu, B. Tang, Elastic stability criteria of seven crystal systems and their application under pressure: taking carbon as an example, J. Appl. Phys. 133 (2023).
[32] S. Baroni, S. De Gironcoli, A. Dal Corso, P. Giannozzi, Phonons and related crystal properties from density-functional perturbation theory, Rev. Mod. Phys. 73 (2001) 515.
[33] M. Warren, G. Ackland, Ab initio studies of structural instabilities in magnesium silicate perovskite, Phys. Chem. Miner. 23 (1996) 107–118.
[34] M.C. Warren, G.J. Ackland, B.B. Karki, S.J. Clark, Phase transitions in silicate perovskites from first principles, Mineral. Mag. 62 (1998) 585–598.
[35] N.W. Ashcroft, N. David Mermin Solid State Physics, Dover Ed, New York, 1976.
[36] O.L. Anderson, A simplified method for calculating the Debye temperature from elastic constants, J. Phys. Chem. Solid. 24 (1963) 909–917.
[37] S. Cheung, W.-Q. Deng, A.C. Van Duin, W.A. Goddard, ReaxFFMgH reactive force field for magnesium hydride systems, J. Phys. Chem. 109 (2005) 851–859.
[38] S. Cui, W. Feng, H. Hu, Z. Feng, Y. Wang, Structural phase transitions in MgH2 under high pressure, Solid State Commun. 148 (2008) 403–405.
[39] M. Durandurdu, New high-pressure phase of MgH2: an ab initio constant-pressure study, Europhys. Lett. 105 (2014) 46001.
[40] S. Kanagaprabha, A. Asvinimeenaatci, R. Rajeswarapalanichamy, K. Iyakutti, First principles study of pressure induced structural phase transition in hydrogen storage material—MgH2, Phys. B Condens. Matter 407 (2012) 54–59.
[41] T. Moriwaki, Y. Akahama, H. Kawamura, S. Nakano, K. Takemura, Structural phase transition of rutile-type MgH2 at high pressures, J. Phys. Soc. Jpn. 75 (2006) 074603.
[42] D. Moser, G. Baldissin, D. Bull, D. Riley, I. Morrison, D. Ross, W. Oates, D. Noréus, The pressure–temperature phase diagram of MgH2 and isotopic substitution, J. Phys. Condens. Matter 23 (2011) 305403.
[43] V. Nayak, U. Verma, Phase transition and optoelectronic properties of MgH2, Phase Transitions 89 (2016) 437–447.
[44] P. Vajeeston, P. Ravindran, B. Hauback, H. Fjellvåg, A. Kjekshus, S. Furuseth, M. Hanfland, Structural stability and pressure-induced phase transitions in MgH 2, Phys. Rev. B Condens. Matter 73 (2006) 224102.
[45] L. Zhang, Y. Wang, T. Cui, Y. Li, Y. Li, Z. He, Y. Ma, G. Zou, Ca Cl 2-type high-pressure phase of magnesium hydride predicted by ab initio phonon calculations, Phys. Rev. B Condens. Matter 75 (2007) 144109.
[46] C. Jensen, K. Gross, Development of catalytically enhanced sodium aluminum hydride as a hydrogen-storage material, Appl. Phys. A 72 (2001) 213–219.
[47] E. Fakioğlu, Y. Yürüm, T.N. Veziroğlu, A review of hydrogen storage systems based on boron and its compounds, Int. J. Hydrogen Energy 29 (2004) 1371–1376.
[48] J.-P. Soulié, G. Renaudin, R. Černý, K. Yvon, Lithium boro-hydride LiBH4: I. Crystal structure, J. Alloys Compd. 346 (2002) 200–205.
[49] A. Züttel, S. Rentsch, P. Fischer, P. Wenger, P. Sudan, P. Mauron, C. Emmenegger, Hydrogen storage properties of LiBH4, J. Alloys Compd. 356 (2003) 515–520.
[50] L. Schlapbach, A. Züttel, Hydrogen-storage materials for mobile applications, Nature 414 (2001) 353–358.
[51] A. Lukacs III, L. Macadams, K. Christmas, Ambient Temperature Liquid Ammonia Process for the Manufacture of Ammonia Borane, Google Patents, 2010.
[52] Y. Suttisawat, P. Rangsunvigit, B. Kitiyanan, S. Kulprathipanja, A reality check on using NaAlH 4 as a hydrogen storage material, J. Solid State Electrochem. 14 (2010) 1813–1819.